Quantum control of entangled photon-pair generation in electron-atom collisions driven by laser-synthesized free-electron wave packets

R. Esteban Goetz [*] and Klaus Bartschat

Department of Physics and Astronomy, Drake University, Des Moines, Iowa 50311, USA

We propose an extension of coherent control using laser-synthesized free-electron matter waves. In contrast to coherent control schemes exploiting optical coherences to steer the dynamics of matter waves, we analyze the opposite and investigate the control of quantum light emission driven by laser-sculpted coherent free-electron matter waves. We apply this concept to the control of entangled photon-pair emission in electron-atom collisions, in which the incident electron wave packet, colliding with a target atom B, is engineered by interferometric resonantly enhanced multiphoton ionization of a parent atom A. Each ionization pathway leads to electron wave packets that coherently interfere during temporal evolution in the continuum. Their mutual coherence can be controlled by adjusting the relative phases or time delays of the frequency components of the ionizing field contributing to the interfering pathways. We report coherent control of entangled photon-pair generation in radiative photocascade emission upon decay of the target atom after inelastic excitation triggered by the collision with the synthesized electron wave packet.

DOI: 10.1103/PhysRevA.103.043112

I. INTRODUCTION

Coherence [1] and quantum interferences [2,3] are the cornerstones of coherent control of photoinduced processes. A prototypical example is two-pathway coherent control of photoionization. It exploits optical coherences to manipulate matter-wave interferences to ultimately steer the ionization dynamics into a desired target outcome. In its simplest form, coherent control of photoionization is achieved by adjusting the relative phase [4–10] or time delay [11,12] between the frequency components of bichromatic fields promoting single- and two-photon ionization. The mutual coherence between both frequency components determines the coherence properties of the released photoelectron wave packet. These are imprinted in the angular distribution of the photoelectron, which has led to its use in the control of photoelectron angular distributions (PADs) [4–9].

An experimental application of the control of free-electron wave-packet interferences consists in shaping the three-dimensional PAD using phase- and polarization-shaped fields. Additional degrees of freedom can be exploited by generalizing the bichromatic scenario to cases comprising a manifold of interfering multiphoton ionization pathways. Recent experimental works on resonantly enhanced multiphoton ionization of potassium atoms using amplitude, phase- and polarization-shaped pulses made it possible to Fourier synthesize free-electron wave packets, i.e., to engineer photoelectron wave packets with tailored momentum distribution, by influencing the mutual coherence among the interfering partial-wave components originating from the various allowed pathways for multiphoton ionization [13–15].

Recalling that these synthesized electron matter waves originate from individual wave packets coherently interfering during their temporal evolution in the continuum [13], the question arises whether such interferences can be coherently manipulated to further control matter-induced processes in a target system.

In this work, we investigate the capabilities of synthesized free-electron wave packets to control dynamical processes in matter-matter interactions. As an application, we review and adapt to a modern contextual technological framework the pioneering works on coincidence detection measurements of entangled photon-pair generation by electron bombardment of a target atom [16] and scrutinize the control of entangled photon-pair generation triggered by the coherent interaction of synthesized free-electron wave packets colliding with a target atom B. The incident photoelectron originates from coherently controlled interferometric multiphoton ionization of its parent atom A, as depicted in Fig. 1(a). It is composed of two individual wave packets originating from each ionization pathway, as illustrated in Fig. 1(b). Both components propagate under the field-free Hamiltonian while coherently interfering in the continuum as they propagate towards the target. Interaction with the latter results in elastic scattering of the incident wave packet and inelastic excitation of the target. We analyze the emission of entangled photon pairs in subsequent radiative photocascade emission from the excited target atom.

Light-driven control of entangled photon-pair states produced by parametric down-conversion is a current topic of active research with major impact in photonic quantum information sciences [17–20]. Control of spontaneous fluorescence (intensity) emission has been reported in single [21–24] and parametric-down photon emission [25] using coherent and chirped light sources and by exploiting the twist phase of a
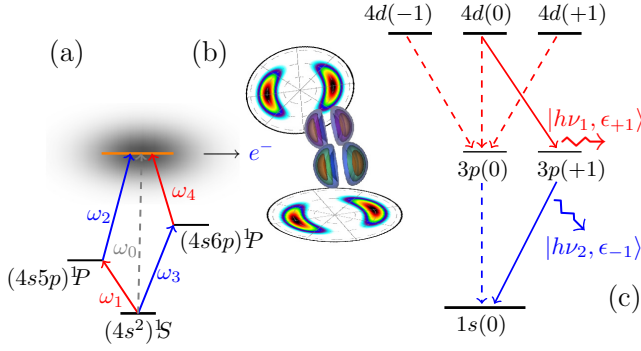
_____
*esteban.goetz@drake.edu

FIG. 1. Matter-wave control of correlated photon-pair generation: (a) Ionization of atom A by a classical field probing a manifold of interfering ionization pathways generates a coherent superposition of continuum states, resulting in (b) a coherent photoelectron wave packet with a tailored momentum distribution. (c) Example of radiative photocascade emission in the target atom B following inelastic excitation induced by the incident photoelectron wave packet.

Gaussian beam with partial transverse spatial coherence [26]. Here, we exploit the use of laser-synthesized electron matter waves to control the correlated angular distribution of entangled photon-pair emission in electron-atom collisions.

II. THEORETICAL MODEL

The atom-photon field interaction is treated at the level of the Weisskopf-Wigner theory for spontaneous emission [27]. Deexcitation of the target atom B occurring during and after collision with the incident electron wave packet yields the photon field in an excited multimode state. The basis,

$$|n_{k_1,\sigma_1}, n_{k_2,\sigma_2}, \dots\rangle = \prod_{k_j,\sigma_j} |n_{k_j,\sigma_j}\rangle, \qquad (1)$$

represents n_{k_j,σ_j} photons in mode (k_j, σ_j) with momentum $\hbar k_j$ and polarization $\hat{\epsilon}_{\sigma_j}$ subject to the transversality conditions $\hat{\epsilon}_{\sigma_j} \cdot k_j = 0$. Atom B and the photon field are coupled via the terms $\hat{\mathbf{A}}_s(\hat{\mathbf{r}}) \cdot \hat{\mathbf{p}}$ and $\hat{\mathbf{A}}_s(\hat{\mathbf{r}}) \cdot \hat{\mathbf{A}}_s(\hat{\mathbf{r}})$, with

$$\hat{\mathbf{A}}_s(\hat{\mathbf{r}}) = \sum_{k_j,\sigma_j} A_0(k_j) \big[\hat{\mathbf{a}}_{k_j,\sigma_j} e^{i k_j \cdot \hat{\mathbf{r}}} \hat{\mathbf{e}}_{\sigma_j} + \hat{\mathbf{a}}^\dagger_{k_j,\sigma_j} e^{-i k_j \cdot \hat{\mathbf{r}}} \hat{\mathbf{e}}_{\sigma_j} \big] \quad (2)$$

as the vector potential operator coupling the eigenstates of B with the photon field. $\hat{\mathbf{a}}^\dagger_{k_j,\sigma_j}$ ($\hat{\mathbf{a}}_{k_j,\sigma_j}$) creates (annihilates) one photon in mode (k_j, σ_j). The Hamiltonian

$$\hat{\mathbf{H}}_{AB}(t) = [\hat{\mathbf{H}}_A - e\hat{\mathbf{r}} \cdot \hat{\mathbf{E}}(\hat{\mathbf{r}}, t)] \otimes \mathbb{1} + \hat{\mathbf{V}}_I$$

$$+ \mathbb{1} \otimes \left\{ \sum_{k_j,\sigma_j} \hbar\omega(k_j) + \frac{1}{2m} \left[\hat{\mathbf{p}} - \frac{e}{c} \hat{\mathbf{A}}_s(\hat{\mathbf{r}}, t) \right]^2 \right\} \quad (3a)$$

dictates the ionization dynamics of atom A, scattering of the resulting photoelectron wave packet by atom B, excitation of the latter due to collision, and photoemission upon deexcitation of atom B. The interaction

$$\hat{\mathbf{V}}_I = V^B_{ne}(\hat{\mathbf{r}} - \mathbf{R}_B) \otimes \mathbb{1} + \hat{\mathbf{V}}_{ee}(\hat{\mathbf{r}}, \hat{\mathbf{r}}') + \mathbb{1} \otimes V^B_{ne}(\hat{\mathbf{r}} - \mathbf{R}_B) \quad (3b)$$

mediates the elastic scattering as well as inelastic excitation of atom B with no change in the distribution of the photon modes. Ionization of atom A is controlled by the classical field $\mathbf{E}(\mathbf{r}, t) = \mathbf{E}(t) f_{\Omega_A}(\mathbf{r})$, with $f_{\Omega_A}(\mathbf{r})$ a Heaviside function. The latter ensures a constant spatial distribution in the vicinity of atom A and leaves the target atom B unaffected. $V^B_{ne}(\hat{\mathbf{r}} - \mathbf{R}_B)$ is the potential energy due to the effective nuclear charge distribution of atom B, with $\mathbf{R}_B$ the (fixed) origin of the coordinates of atom B and $\hat{\mathbf{V}}_{ee}(\hat{\mathbf{r}}, \hat{\mathbf{r}}')$ the potential-energy interaction between the incident electron and the electron in the target. To simplify the notation, Eq. (3a) is written in the effective tensor product basis $|\psi^A_{\gamma_a}\rangle \otimes |\tilde{\psi}^B_{\gamma_b}\rangle$, where $|\tilde{\Phi}^B_{\gamma_B}\rangle \equiv |\Phi^B_{\gamma_B}\rangle \otimes |n_{k_1,\sigma_1}, n_{k_2,\sigma_2}, \dots\rangle$, with $|\Phi^A_{\gamma_A}\rangle$ and $|\Phi^B_{\gamma_B}\rangle$ as the eigenvectors of the isolated Hamiltonians, $\hat{\mathbf{H}}_A$ and $\hat{\mathbf{H}}_B$, of atoms A and B, respectively, satisfying $\hat{\mathbf{H}}_A |\Phi^A_{\gamma_a}\rangle = \epsilon^A_{\gamma_a} |\Phi^A_{\gamma_a}\rangle$ and $\hat{\mathbf{H}}_B |\Phi^B_{\gamma_b}\rangle = \epsilon^B_{\gamma_b} |\Phi^B_{\gamma_b}\rangle$. With this contracted notation, the first term on the right-hand side of Eq. (3a) applied to an element, e.g., $|\Phi^A_{\gamma_A}\rangle \otimes |\tilde{\Phi}^B_{\gamma_B}\rangle$, will effectively only act on $|\Phi^A_{\gamma_A}\rangle$, leaving the component $|\tilde{\Phi}^B_{\gamma_B}\rangle$ unaltered. Conversely, the third term (second line) in Eq. (3a) acts on $|\tilde{\Phi}^B_{\gamma_B}\rangle$, leaving the component $|\Phi^A_{\gamma_A}\rangle$ unchanged. The same applies to Eq. (3b), where $\hat{\mathbf{r}}'$ and $\hat{\mathbf{r}}$ in $\hat{\mathbf{V}}_{ee}(\hat{\mathbf{r}}, \hat{\mathbf{r}}')$ are used to symbolize a two-electron potential-energy operator, in contrast to the one-electron operators in the first and third terms; see the Appendices.

We solve the time-dependent Schrödinger equation

$$i\frac{\partial}{\partial t}|\Psi_S(t)\rangle = \hat{\mathbf{H}}_{AB}(t)|\Psi_S(t)\rangle, \qquad (4a)$$

and write $|\Psi_S(t)\rangle$ as a coherent superposition in the antisymmetrized tensor product space spanned by the eigenvectors of the isolated Hamiltonians and Eq. (1), i.e.,

$$|\Psi_S(t)\rangle = \sum_{\gamma^A_a, \gamma^B_b} \sum_{n_{k_1,\sigma_1}} \sum_{n_{k_2,\sigma_2}} \cdots |\Phi_{\gamma^A_a, \gamma^B_b}\rangle \otimes \prod_{k_j,\sigma_j} |n_{k_j,\sigma_j}\rangle$$

$$\times \exp\left[-i\left(\epsilon^A_{\gamma_a} + \epsilon^B_{\gamma_b} + \sum_{k_i,\sigma_i} \omega(k_i) n_{k_i,\sigma_i} \right) t \right]$$

$$\times S_{\gamma^A_a, \gamma^B_b}(n_{k_1,\sigma_1}, n_{k_2,\sigma_2}, n_{k_3,\sigma_3} \dots; t). \qquad (4b)$$

The vector $|\Phi_{\gamma^A_a, \gamma^B_b}\rangle \equiv |\Phi^A_{\gamma^A_a}\rangle \otimes |\Phi^B_{\gamma^B_b}\rangle - |\Phi^B_{\gamma^B_b}\rangle \otimes |\Phi^A_{\gamma^A_a}\rangle$ represents one electron in a spin-orbital state $\langle \mathbf{r}_1; m_{s_1}|\Phi^A_{\gamma^A_a}\rangle$ of A and the other one in $\langle \mathbf{r}_2; m_{s_2}|\Phi^B_{\gamma^B_b}\rangle$ of B, with $m_{s_{1,2}}$ the spin-magnetic quantum numbers for electrons 1 and 2. Note that $\langle \mathbf{r}_1, m_{s_1}; \mathbf{r}_2, m_{s_2}|\Phi_{\gamma^A_a, \gamma^B_b}\rangle = -\langle \mathbf{r}_2, m_{s_2}; \mathbf{r}_1, m_{s_1}|\Phi_{\gamma^A_a, \gamma^B_b}\rangle$. Summation over γ^A_a includes all bound and continuum states, and $\omega(k_j) = |k_j| c$. Matrix elements to describe the ionization process were obtained with the B-spline R-matrix codes [28].

Due to the many-body character of the stimulated photon field, a full time-dependent treatment of the dynamics, while keeping track of every possible photon mode emitted and absorbed during the aforementioned processes, is a formidable and computationally prohibitive task. To scrutinize the control mechanisms for radiative photon-cascade emission triggered by the collision while keeping the calculations tractable, we resort to obtain the time-dependent coefficients in Eq. (4b)
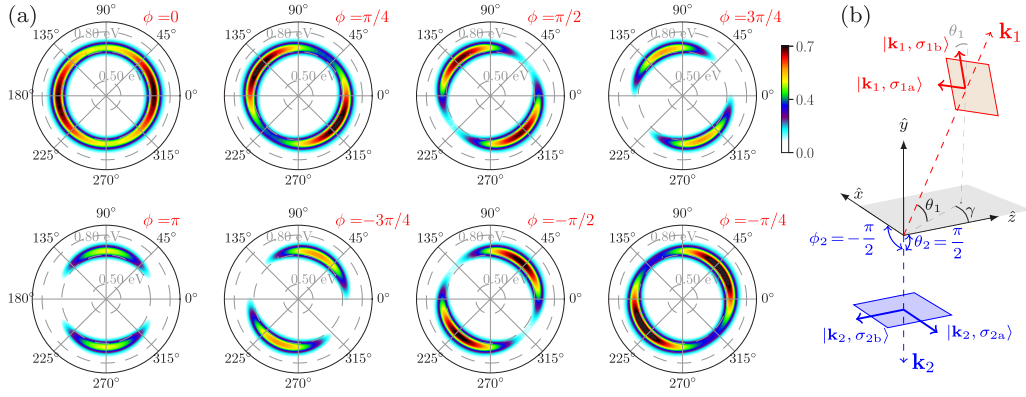
FIG. 2. Inelastic excitation-decay control mechanism: (a) Angular distribution of correlated photon-pair emission as a function of the relative phase, ϕ, between the laser frequencies ω_1 and ω_3 shown in Fig. 1(a). The incident photoelectron wave packet results from a coherent superposition of even-parity two-photon ionization pathways. Note that the angular probability of photodetection follows the relative phase. (b) Correlated photon-pair detection scheme discussed in the text ($\gamma = 0$).

from a time-dependent perturbative series expansion up to order k. Details are provided in the Appendices.

III. ANGLE-RESOLVED COINCIDENCE PHOTODETECTION SCHEME

We start by considering resonantly enhanced two-pathway coherent ionization of Ca as schematically depicted in Fig. 1(a). Resonant excitation of the $(4s5p)\,^1P$ and $(4s6p)\,^1P$ states is mediated by the frequency components $\omega_1 = 4.554$ eV and $\omega_3 = 5.167$ eV of a classical field, with both left-circularly polarized. Their relative phase is used as a control parameter. Ionization is ensured by the linearly polarized frequency components $\omega_2 = 17.324$ eV and $\omega_4 = 16.721$ eV with a flat spectral phase. The frequency components have a duration of 20 fs (FWHM) and are not time delayed. Each ionization pathway generates a coherent superposition of scattering eigenstates of A peaked at the same photoelectron energy of 15.755 eV, as depicted in Fig. 1(b). The angular-momentum components defining the wave packets that arise from each of these ionization channels are coherently combined, carrying the temporal coherence of the classical field.

The target atom B, initially in its ground state, is taken as the hydrogen atom. The quantization axis is defined by the vector parallel to the $\hat{z}$ direction connecting both atoms, situated at the positions $\boldsymbol{R}_A$ and $\boldsymbol{R}_B$ with $|\boldsymbol{R}_B - \boldsymbol{R}_A| = R_{B,z} - R_{A,z} = 1200$ atomic units. After excitation by the tailored electron wave packet, optical decay may occur via different deexcitation pathways allowed by selection rules, as epitomized in Fig. 1(c).

The angular distribution of the emitted photons is obtained using the multipole expansion in Eq. (2),

$$e^{\pm i k_j \cdot \mathbf{r}} = 4\pi \sum_{\lambda, \mu} (\pm i)^\lambda j_\lambda(k_j r) Y_\mu^\lambda(\theta_r, \phi_r) Y_\mu^{\lambda *}(\theta_{k_j}, \phi_{k_j}), \quad (5)$$

with the spherical harmonics $Y_\mu^\lambda(\theta_{k_j}, \phi_{k_j})$ for the angles of photoemission defining the mode $(\mathbf{k}_j, \sigma_j)$. The polarization components of the emitted photons are obtained according to $\hat{e}_{\sigma_{ja}} = k_j \times \hat{e}_0 / |k_j \times \hat{e}_0|$ and $\hat{e}_{\sigma_{jb}} = k_j \times \hat{e}_{\sigma_{ja}} / |k_j \times \hat{e}_{\sigma_{ja}}|$,

where

$$k_j = (4\pi/3)^{1/2} \, |k_j| \sum_{q=0, \pm 1} Y_q^1(\theta_{k_j}, \phi_{k_j}) \hat{e}_q^*, \quad (6)$$

with $\hat{e}_q$ the covariant spherical unit vectors. Both polarization vectors are functions of the angles $(\theta_{k_j}, \phi_{k_j})$.

The coincidence photodetection scheme is shown in Fig. 2(b): a photodetector $\mathcal{D}_2$, fixed at $\theta_{k_2} = \pi/2$ and $\phi_{k_2} = -\pi/2$, registers polarization- and wavelength-filtered photons with energy $h\nu_2 = 12.078$ eV, corresponding to the energy of the transitions $3p(m = \pm 1, 0) \to 1s$ in Fig. 1(c). $\mathcal{D}_2$ is set to register only the wavelength-filtered photons that are linearly polarized along the z direction in Fig. 2(b) (blue color). Detection by $\mathcal{D}_2$ therefore maps the second step of the radiative cascade decay defined by the $3p(0) \to 1s$ transition in Fig. 1(c). The state of such photon is hereafter referred to as mode (2).

A second detector $\mathcal{D}_1$, fixed at $\phi_{k_1} = \pi/2$ but free to move along the polar coordinate θ_{k_1}, scans, along θ_{k_1}, the direction of emission of the correlated peer defined by the state $|\mathbf{k}_1, \sigma_{1b}\rangle$ in Fig. 2(b) (red color): a photon of energy $h\nu_1 = 0.661$ eV, corresponding to the energy of the radiative transition $4d(\{m\}) \to 3p(\pm 1, 0)$ in Fig. 1(c). The orthogonal polarization components, σ_{1a} and σ_{1b}, of the photon emitted in the first step of the cascade fulfilling the transversality condition are depicted in Fig. 2(b) (red color). Note that these components are correlated to that of the photon registered by $\mathcal{D}_2$. Finally, as it scans θ_{k_1}, $\mathcal{D}_1$ is set to register only the wavelength-filtered photons with the polarization component along the direction $\hat{e}_{\sigma_{1b}}$ depicted in Fig. 2(b) (red color). Explicit expressions for $\hat{e}_{\sigma_{1a}}$ and $\hat{e}_{\sigma_{1b}}$ as a function of the emission angles $(\theta_{k_1}, \phi_{k_1})$ are given in Eq. (C6) of Appendix C, Sec. C 1 a.

IV. ANGLE-RESOLVED PHOTON-PAIR EMISSION: NUMERICAL RESULTS

Figure 2(a) shows the angular probability distribution of measuring the correlated photon in coincidence with its correlated peer in mode (2) as a function of the relative phase between the frequencies ω_1 and ω_3 of Fig. 1(a). The direction
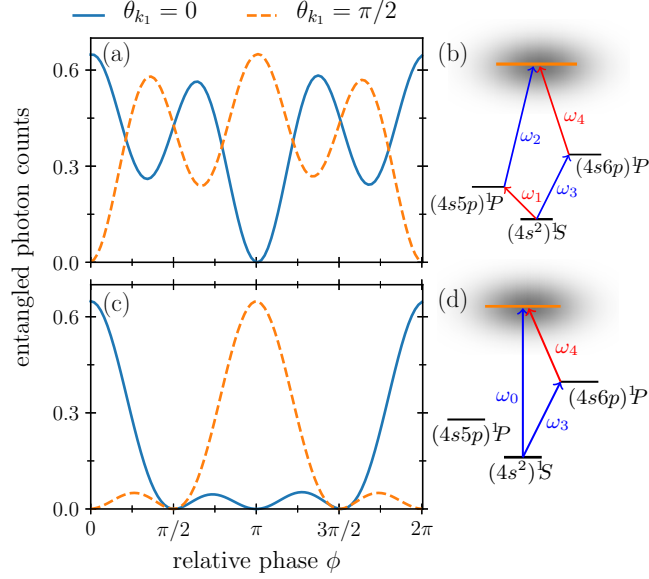
FIG. 3. (a) Photodetection probability at angles $\theta_{k_1} = 0$ (solid blue line) and $\theta_{k_1} = \pi/2$ (dashed orange line) as a function of the relative phase between the laser frequencies ω_1 and ω_3 shown in (b) when a photon in mode (2) is simultaneously detected. The incident electron wave packet originates from the ionization scheme shown in (b). (c) Same as (a), but as a function of the relative phase between the laser frequencies ω_0 and ω_3 shown in (d).

of emission exhibits a noticeable dependence on the temporal coherence conveyed by the incident photoelectron wave packet: the probability of entangled photon-pair detection is strongly affected by the mutual phase of the photoionization probability amplitudes, controlled by the relative phase between the frequency components of the classical field probing the contributing photoionization pathways.

The angle-resolved occurrence of coincident photodetection is also sensitive to the parity of the photoionization pathways probed to engineer the incident photoelectron wave packet. This is shown in Fig. 3, comparing, at the fixed emission angles $\theta_{k_1} = 0$ and $\theta_{k_1} = \pi/2$, the probability of coincident photodetection already discussed in Fig. 2, this time using different photoionization schemes to engineer the incident electron wave packet: same- and opposite-parity photoionization pathways.

Figure 3(a) displays the probability of coincident photodetection obtained when the incident photoelectron wave packet is engineered according to the resonantly enhanced two-photon ionization scheme promoting even-parity pathways depicted in Fig. 3(b). As shown in Fig. 3(a), the probability for simultaneous photon-pair detection at a given direction θ_{k_1} can be entirely suppressed or enhanced depending on the relative phase between the contributing photoionization pathways.

Likewise, as shown in Fig. 3(c), opposite-parity photoionization pathways, as depicted in Fig. 3(d), can also be exploited to engineer the photoelectron wave packet to ultimately suppress or enhance the probability of correlated photon-pair detection. In this case, control is achieved by manipulating the relative phase between the one- and two-photon

ionization pathways through the relative phase between the frequencies ω_0 and ω_3.

As defined, the relative phase corresponding to $\phi = 0$ maximizes (minimizes) the probability of detection in the direction $\theta_{k_1} = 0$ ($\theta_{k_1} = \pi/2$) for both photoionization schemes depicted in Figs. 3(b) and 3(d) when a photon in mode (2) is simultaneously detected. Conversely, for $\phi = \pi$, the probability of detection in the direction $\theta_{k_1} = 0$ ($\theta_{k_1} = \pi/2$) is minimized (maximized) for both schemes. In contrast, the relative phases corresponding to $\phi = \pi/2$ and $\phi = 3\pi/2$ result in the suppression of photon-pair coincident detection at angles $\theta_{k_1} = 0$ and $\theta_{k_1} = \pi/2$ for the case of an odd-even parity photoionization pathway [cf. Fig. 3(c)], whereas its even-parity counterpart results in an equal probability of coincidence photodetection [cf. Fig. 3(a)].

Control of directional correlated photon-pair detection can also be achieved by adjusting the relative time delays between the different pulses carrying the various frequency components in Fig. 1(a). To illustrate this, we choose two pump-laser frequencies, ω_1 and ω_3, to resonantly excite the $(4s5p)\,^1P$ and $(4s6p)\,^1P$ states in atom A, creating a superposition of states evolving according to the free-field Hamiltonian. After a delay τ, a probe field with frequencies ω_2 and ω_4 is introduced, ionizing the electron in the coherent superposition. The resulting photoelectron wave packet then carries the coherence of the superposition of bound states, defined by the phase accumulated between the pump and probe pulses. Figure 4 shows the time-resolved probability of correlated photon-pair detection as a function of the delay τ. The probability for coincident photodetection upon sequential deexcitation of atom B, located far from atom A, is sensitive to the phase of the coherent superposition state in atom A, carried by the colliding photoelectron wave packet. For a fixed direction θ_{k_1}, the photon yield can be controlled significantly. Compare, for example, the yields at $\theta_{k_1} = 45°$ for the delays $\tau = -50$ and $\tau = -40$ fs.

V. CORRELATED PHOTON-PAIR EMISSION: CONTROL MECHANISM

A. Coherent radiative cascade-decay dynamics

If only the $4d(0)$ state were inelastically excited by the incident photoelectron wave packet, the radiative cascade transition given by, e.g., $4d(0) \rightarrow 3p(1) \rightarrow 1s$ [cf. solid (red and blue) lines in Fig. 1(c)] could be mapped by setting $\mathcal{D}_2$ to detect wavelength- and polarization-filtered left-circularly polarized photons only (with energy $h\nu_2$ as usual), while setting $\mathcal{D}_1$ for coincidence detection of right-circularly ($\hat{\mathbf{e}}_{\sigma_1} = \hat{\boldsymbol{\epsilon}}_{+1}$) polarized photons with energy $h\nu_1$. A measurement by $\mathcal{D}_2$ then provides the complete information about the polarization state of the photon emitted in the first step in the cascade. More explicitly, the "which pathway information" related to the emission of the photon with energy $h\nu_1$ can be determined by $\mathcal{D}_2$. Consequently, the angular distribution of photons detected by $\mathcal{D}_1$ exhibits no sensitivity as a function of the phase of the $4d(0)$ state. All features of the angular distribution of photons registered by $\mathcal{D}_1$ are then solely dictated by the transversality condition $\hat{\mathbf{e}}_{\sigma_1} \cdot \mathbf{k}_1 = 0$.
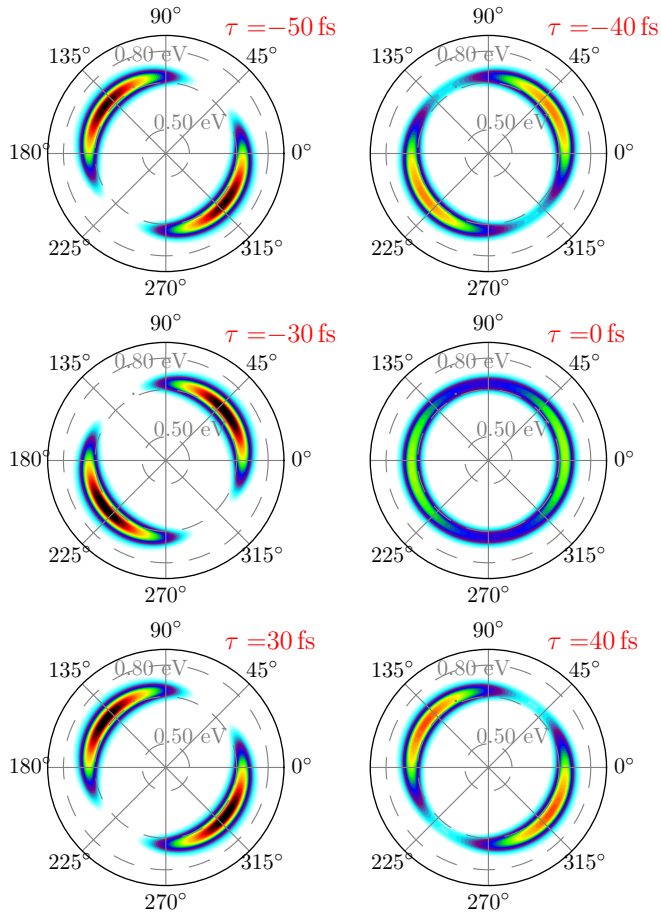
FIG. 4. Time-resolved probability for coincident photodetection as a function of the time delay between the pump and probe pulses discussed in the text. Color map as in Fig. 2.

Conversely, if $\mathcal{D}_2$ is set to register linearly polarized photons only (along the $\hat{z}$ direction) with energy $h\nu_2$ as usual, then only detection of linearly polarized photons with energy $h\nu_1$ by $\mathcal{D}_1$ gives nonvanishing coincidence counts, mapping the pathway $4d(0) \rightarrow 3p(0) \rightarrow 1s$. Likewise, if the state $4d(-1)$ [$4d(+1)$] is *solely populated*, the coincidence detection is restricted to the case involving circularly polarized right [left] photons with energy $h\nu_1$ and the linearly polarized photons by $\mathcal{D}_2$. In either case, detection by $\mathcal{D}_2$ unambiguously determines the deexcitation pathways involved in the emission of the photon registered by $\mathcal{D}_1$. As before, the angular distribution of photons detected by $\mathcal{D}_1$ is dictated by the transversality condition and cannot be coherently controlled.

Keeping the same detection configuration for $\mathcal{D}_2$, a more interesting case occurs when the inelastic excitation triggered by the incident electron wave packet leaves the target atom in a coherent superposition with several states coherently excited. In striking contrast to the previous cases, the deexcitation pathway associated with the emission of a photon with energy $h\nu_1$ can no longer be unambiguously determined by $\mathcal{D}_2$ alone: the photon with energy $h\nu_1$ can be, e.g., circularly right [$4d(-1) \rightarrow 3p(0) \rightarrow 1s$], left [$4d(1) \rightarrow 3p(0) \rightarrow 1s$], or linearly [$4d(0) \rightarrow 3p(0) \rightarrow 1s$] polarized.

Each of these configurations results in a specific angular distribution registered by $\mathcal{D}_1$. While the *which pathway information* can be restored by setting $\mathcal{D}_1$ to register only those photons with the polarization of interest, this is no longer the case if the polarization component of detection, $\hat{\mathbf{e}}_{\sigma_{1b}}$ in Fig. 2(b), is chosen in such a way that several deexcitation pathways $4d(m) \rightarrow 3p(0)$ can contribute. In this case, a unique deexcitation path leading to the $3p(0)$ state can no longer be unambiguously determined: several pathways can contribute to the cascade $4d(m) \rightarrow 3p(0) \rightarrow 1s$. Correspondingly, the angular distribution of photons registered by $\mathcal{D}_1$ contains coherent contributions of angular-momentum components of photons arising from the possible pathways $4d(m) \rightarrow 3p(0)$ [cf. Fig. 1(c) (dashed lines)], if these components contribute to the same photon mode $|k_1, \sigma_{1b}\rangle$. Among all possible pathways contributing to $|k_1, \sigma_{1b}\rangle$, only those decaying through the $3p(0)$ state will coherently contribute to the coincidence detection, as $\mathcal{D}_2$ is set to only register linearly polarized photons. The conditions for quantum interference are then fulfilled, as several deexcitation pathways lead to the same final quantum state.

The positions of the maxima and minima in Fig. 2(a) are dictated by the transversality condition for the mode $|k_1, \sigma_{1b}\rangle$ and the magnetic quantum number m of the $4d(m)$ state involved in the deexcitation transition to the $3p(0)$ state. The photon with energy $h\nu_1$ is linearly polarized, i.e., parallel to the $\hat{z}$ axis in Fig. 2(b), if the transition $4d(0) \rightarrow 3p(0)$ takes place. In this case, the maxima correspond to $\theta_{k_1} = 90°$ and $\theta_{k_1} = 270°$, since σ_{1b} is along the $\hat{z}$ direction. The minima correspond to the angles $\theta_{k_1} = 0°$ and $\theta_{k_1} = 180°$, since σ_{1b} is then perpendicular to the $\hat{z}$ axis of polarization: $\mathcal{D}_1$ registering photons with polarization component along σ_{1b}, then parallel to the $\hat{y}$ axis, finds no signal. Conversely, if the transition $4d(\pm 1) \rightarrow 3p(0)$ takes place, then the photon is circularly polarized, and the aforementioned positions for the maxima and minima are inverted.

Correspondingly, when the target atom is in a coherent superposition with a manifold of $4d(m)$ states populated, deexcitation pathways of the type $4d(m) \rightarrow 3p(0) \rightarrow 1s$ may contribute to the same photon modes registered in coincidence by $\mathcal{D}_1$ and $\mathcal{D}_2$. As previously discussed, the angle-resolved probability of correlated photon-pair emission contains coherent contributions from each of these deexcitation pathways, as long as these lead the overall system to the same final quantum state, complying with the conditions for quantum pathway interference. Consequently, the positions of the maxima and minima are sensitive to the phases of the $4d(m)$ states. As observed in Figs. 2(a) and 4, they fluctuate between the limiting values obtained when only one $4d(m)$ state is populated.

B. Coherent inelastic excitation dynamics

As alluded to above, control over the angle-resolved probability of photocascade emission observed in Figs. 2, 3, and 4 is achieved by controlling the aforementioned quantum interferences leading to the same overall final quantum state. More specifically, this involves manipulating interferences between the relevant angular-momentum components contributing to the same photon mode $|k_1, \sigma_{1b}\rangle$ for the radiative cascade decay $4d(m) \rightarrow 3p(0) \rightarrow 1s$. Control is achieved by influencing the

relative phase of the relevant $4d(m)$ states in the coherent superposition in the target atom contributing to the cascade.

To rationalize how the incident wave packet exerts control over the phases in the coherent superposition, it is convenient to consider the states of the incident and target electrons before and after their mutual interaction. To simplify the discussion and for general orientation only, we shall neglect in the following discussion the photon field and exchange terms. A more involved and complete description can be found in the Appendices. Then the probability amplitude for inelastic excitation to the final states $|\Phi_{\boldsymbol{p}_a'}^A\rangle$ and $|\Phi_{\gamma_b'}^B\rangle$ for the incident and target electrons, respectively, is given, to the lowest order, by

$$
C(\boldsymbol{p}_a', \gamma_{b'}^B; t) = -i \sum_{k=1}^{2} \int d\boldsymbol{p}_a^A \langle \Phi_{\boldsymbol{p}_a'^A}^A; \Phi_{\gamma_{b'}^{/B}}^B | \hat{\boldsymbol{V}}_{ee} | \Phi_{\boldsymbol{p}_a'}^A; \Phi_{\gamma_b^o}^B \rangle
$$
$$
\times \int_{-\infty}^{t} c_{\boldsymbol{p}_a}^{(w)}(t') e^{i(\epsilon_{\boldsymbol{p}_a'}^A + \epsilon_{\gamma_b'}^B - \epsilon_{\boldsymbol{p}_a}^A - \epsilon_{\gamma_b^o}^B)t'} dt', \quad (7)
$$

with $\epsilon_{\gamma_b^o}^B$ ($\epsilon_{\gamma_{b'}}^B$) the initial (final) energy associated with the initial (final) state, $|\Phi_{\gamma_b^o}^B\rangle$ ($|\Phi_{\gamma_{b'}}^B\rangle$), of the target electron, initially in the ground state $|\Phi_{\gamma_b^o}^B\rangle$. Furthermore, $\epsilon_{\boldsymbol{p}_a}^A$ ($\epsilon_{\boldsymbol{p}_a'}^A$) denotes the initial (final) energy of the incident (scattered) electron wave packet, and $\hat{\boldsymbol{V}}_{ee}$ is the potential-energy operator describing their mutual electrostatic interaction.

The resonantly enhanced two-pathway ionization of atom A dictates the spectral amplitude distribution $c_{\boldsymbol{p}_a}(t)$ of the incident electron wave packet. To proceed with our discussion, $c_{\boldsymbol{p}_a}(t)$ in Eq. (7) is approximated by its asymptotic form in the absence of atom B, i.e., $c_{\boldsymbol{p}_a}^{(w)}(t' \to \infty)$ in Eq. (8), thus describing an electron wave packet arriving from the remote past, similarly to the standard treatment of inelastic scattering by a plane wave. The first-order correction ($w = 1$) reads

$$
c_{\boldsymbol{p}_a}^{(1)}(t) = i \sum_j \langle \Phi_{\boldsymbol{p}_a}^A | \hat{\boldsymbol{d}} | \Phi_{\gamma_a^o}^A \rangle \cdot \boldsymbol{e}^{(j)} \int_{-\infty}^{t} e^{i(\epsilon_{\boldsymbol{p}_a}^A - \epsilon_{\gamma_a^o}^A)t'} E_j(t') dt',
$$
$$
(8a)
$$

with $\hat{\boldsymbol{d}}$ the dipole operator weighted with the spatial Heaviside step function $f_{\Omega_A}(\boldsymbol{r})$ and $|\Phi_{\gamma_a^o}^A\rangle$ the ground state of atom A. The summation is carried out over the frequency components of the ionizing field, indexed by the labels j, polarized in the $\boldsymbol{e}^{(j)}$ direction with respect to the quantization axis $(\boldsymbol{R}_B - \boldsymbol{R}_A)/|\boldsymbol{R}_B - \boldsymbol{R}_A|$. Correspondingly, the second-order correction ($w = 2$) reads

$$
c_{\boldsymbol{p}_a}^{(2)}(t) = -\sum_{\gamma_a^A} \sum_{j,j'} \boldsymbol{e}^{(j)} \cdot \langle \Phi_{\boldsymbol{p}_a}^A | \hat{\boldsymbol{d}} | \Phi_{\gamma_a^A}^A \rangle \langle \Phi_{\gamma_a^A}^A | \hat{\boldsymbol{d}} | \Phi_{\gamma_a^o}^A \rangle \cdot \boldsymbol{e}^{(j')}
$$
$$
\times \int_{-\infty}^{t} e^{i(\epsilon_{\boldsymbol{p}_a}^A - \epsilon_{\gamma_a^A}^A)t'} E_j(t') dt' \int_{-\infty}^{t'} e^{i(\epsilon_{\gamma_a^A}^A - \epsilon_{\gamma_a^o}^A)\tau} E_{j'}(\tau) d\tau.
$$
$$
(8b)
$$

For the case corresponding to the resonantly enhanced two-photon ionization of Fig. 1(a), this can be recast into two individual electron wave packets arising from each ionization pathway and interfering at a common energy $\epsilon_{\boldsymbol{p}_a}^A$ and momentum $\boldsymbol{p}_a$. From Eq. (8), it is apparent that the spectral coherence in the incident photoelectron wave packet, contained in the

coefficients $c_{\boldsymbol{p}_a}^{(w)}$, can be controlled, for example, by adjusting the spectral phases of the ionizing fields $E_j(t)$ contributing to the interfering ionization pathways. In turn, it immediately follows from Eq. (7) that the relative phases associated with the angular-momentum components carried by each of the two partial electron wave packets can coherently influence the population of the states $|\Phi_{\gamma_b'}^B\rangle$ in the target. While inelastic excitation mediated by these angular-momentum components is dictated by the selection rules arising from the matrix elements in Eq. (7), coherent control over the inelastic excitation, on the other hand, will be achieved if at least two inelastic channels leave the quantum system in the same final (excited) state. This is ensured by the individual photoelectron wave packets originating from each photoionization pathway, inelastically exciting the same final state $|\Phi_{\gamma_b'^B}^B\rangle$ with different phases. Consequently, the relative phases of the $4d(m)$ states can be adjusted by coherently tailoring the incident electron wave packet through interfering multiphoton ionization, which in turn influences the coherent deexcitation dynamics and corresponding photocascade emission.

VI. CONCLUSIONS

Motivated by the recent developments in free-electron wave-packet interferometry and engineering, and the increasingly active research in coherent control of entangled photon-pair generation, we investigated the control of angular distributions of correlated photon pairs emitted after electron-atom collisions. In contrast to standard approaches, we demonstrated the possibility of controlling quantum light by employing engineered matter waves. Using calcium and hydrogen as prototypes to control two-photon cascade emission triggered by electron-atom collisions, we demonstrated that laser-synthesized free-electron matter waves can be used to coherently control processes in matter-matter interactions. The tailored electron wave packet is engineered by exploiting interfering multiphoton-ionization pathways, and its coherence properties are controlled by adjusting the spectral phase of the ionizing field. The mutual coherence carried by the individual electron wave packets arising from each ionization pathway are in turn exploited to coherently control the inelastic excitation dynamics in the target atom. Such control ultimately dictates the underlying deexcitation dynamics in the target and corresponding radiative cascade emission. Control over the angle-resolved correlated photon-pair emission demands coherent manipulation of the different deexcitation pathways yielding the overall *electron-target-atom-photon-field system* to the same final quantum state or, equivalently, manipulation of the quantum interferences between the different cascade deexcitation pathways contributing to the same photon modes registered in coincidence detection by the detectors $\mathcal{D}_1$ and $\mathcal{D}_2$. The angle-resolved correlated photon-pair emission is then sensitive to the phases of the inelastically excited states. These are controlled by adjusting the coherence properties of the laser-synthesized photoelectron wave packet. The sensitivity in the correlated angular distribution for the photon modes registered in coincidence detection on the ionizing laser field spectral phase

is a manifestation of quantum interferences in electron-atom collisions.

Taking advantage of coherently driven electron-electron interactions to induce, e.g., population transfers may be beneficial when the efficiency to accomplish the same task using light sources is restricted by electric dipole selection rules. Our results can be extended to more complex cases, such as chiral molecules, with the potential to reveal further insights into the interaction of quantum light with chiral matter waves. We also foresee extending our approach to electron-ion collisions to investigate the control of correlated photon-pair emission after capture of the incident coherent electron wave packet by the target ion.

ACKNOWLEDGMENT

APPENDIX A: HAMILTONIAN SYSTEM

1. Isolated hamiltonians

In order to keep the calculations tractable, we consider two initially isolated, noninteracting atomic systems, labeled A and B, with Hamiltonians

$$\hat{\mathbf{H}}_A = \sum_{i=1}^{N_A} \left(\frac{\hat{\mathbf{p}}_i^2}{2m} + V_{ne}^A(\hat{\mathbf{r}}_i - \hat{\mathbf{R}}_A) + \sum_{i'>i}^{N_A} V_{ee}(\hat{\mathbf{r}}_i - \hat{\mathbf{r}}_{i'}) \right),$$

(A1a)

corresponding to that of the atom from which the photoelectron wave packet is released, and

$$\hat{\mathbf{H}}_B = \sum_{j=1}^{N_B} \left(\frac{\hat{\mathbf{p}}_j^2}{2m} + V_{ne}^B(\hat{\mathbf{r}}_j - \hat{\mathbf{R}}_B) + \sum_{j'>j}^{N_B} V_{ee}(\hat{\mathbf{r}}_j - \hat{\mathbf{r}}_{j'}) \right) \quad \text{(A1b)}$$

for the target atom. They fulfill $\hat{\mathbf{H}}_A|\Phi_{\gamma_a^A}^A\rangle = \epsilon_{\gamma_a}^A|\Phi_{\gamma_a^A}^A\rangle$ and $\hat{\mathbf{H}}_B|\Phi_{\gamma_b^B}^B\rangle = \epsilon_{\gamma_b}^B|\Phi_{\gamma_b^B}^B\rangle$ with eigenvalues $\epsilon_{\gamma_a}^A$ ($\epsilon_{\gamma_b}^B$), where γ_a^A (γ_b^B) collectively denotes a set of quantum numbers that uniquely defines the states $|\Phi_{\gamma_a^A}^A\rangle$ and $|\Phi_{\gamma_b^B}^B\rangle$. The summations are over the N_A and N_B electrons of atoms A and B, respectively. $\hat{\mathbf{V}}_{ee}$ is the electron-electron potential-energy operator, and $\hat{\mathbf{R}}_A$ ($\hat{\mathbf{R}}_B$) is the position operator acting on the nuclear wave function of A (B).

Recoil is not considered. The origins of the coordinate systems are $\mathbf{R}_{0,A}$ ($\mathbf{R}_{0,B}$), defined by the (fixed) position of the pointlike nuclear charge distribution assumed to be of the form $Z_A \delta(\mathbf{R} - \mathbf{R}_A)$ [$Z_B \delta(\mathbf{R} - \mathbf{R}_B)$], with Z_A (Z_B) as the effective nuclear charge. The distance $|\mathbf{R}_A - \mathbf{R}_B|$ is taken such that $\langle \Phi_{\gamma_a^A}^A | \Phi_{\gamma_b^B}^B \rangle = 0$ for all bound states considered. For the numerical calculations, we have set $|\mathbf{R}_B - \mathbf{R}_A| = R_{B,z} - R_{A,z} = 1200$ atomic units. This axis of quantization defines the frame for the electric-field polarization given in Sec. A 2. We denote by $\mathcal{H}_A$ and $\mathcal{H}_B$ the Hilbert spaces spanned by the eigenvectors of the Hamiltonians defined in Eqs. (A1a) and (A1b), respectively.

2. Optical preparation and laser-induced ionization

The optical preparation and ionization of atom A is mediated by a classical field $E(\mathbf{r}, t)$ parameterized as

$$\mathbf{E}(\mathbf{r}, t) = \sum_{\mu_0} \sum_{n=1}^{N} h_{\mu_0}^{(n)}(t - \tau_n) \operatorname{Re}\{e^{-i\Phi_n(t-\tau_n)} \mathbf{e}_{\mu_0}\} f_{\Omega_A}(r),$$

(A2)

with N frequency components ω_n and instantaneous frequencies $\Phi_n(t) = \omega_n t + \tilde{\varphi}_n$, where $\tilde{\varphi}_n = -\omega_n \tau_n + \phi_n$ is the spectral phase, ϕ_n the carrier envelope phase (CEP), and τ_n the time delay with respect to $t = 0$. $h^{(n)}(t - \tau_n)$ is a Gaussian function with adjustable amplitude centered around τ_n. Left-circular [$\mathbf{e}_{-1} = (\mathbf{e}_x - i\mathbf{e}_y)/\sqrt{2}$], right-circular [$\mathbf{e}_{+1} = -(\mathbf{e}_x + i\mathbf{e}_y)/\sqrt{2}$], and linear ($\mathbf{e}_0 = \mathbf{e}_z$) polarization states are described by $\mathbf{e}_{\mu_0}$. The photoelectron wave packet resulting from ionization of A is controlled by means of these field parameters.

To avoid treating the collision dynamics in the presence of a dressing background field, the Heaviside function $f_{\Omega_A}(r)$ ensures a constant amplitude for the spatial distribution of $\mathbf{E}$ within the region defined by the extension of the outermost excited state of atom A. Being zero elsewhere, the target atom B is not affected by the field.

APPENDIX B: EQUATIONS OF MOTION

1. Perturbation expansion

To illustrate our idea of coherent control at a reduced computational cost, we treat the ionization of atom A (here, calcium) and the collision of the resulting photoelectron wave packet with the target atom B (here, atomic hydrogen) as an effective two-electron problem. The Hamiltonian

$$\hat{\mathbf{H}}_{AB}(t) = [\hat{\mathbf{H}}_A - e\,\hat{\mathbf{r}} \cdot \hat{\mathbf{E}}(\hat{\mathbf{r}}, t)] \otimes \mathbb{1} + \hat{\mathbf{V}}_I$$
$$+ \mathbb{1} \otimes \left\{ \sum_{k_j, \sigma_j} \hbar\omega(k_i) + \frac{1}{2m}\left[\hat{\mathbf{p}} - \frac{e}{c}\hat{\mathbf{A}}_s(\hat{\mathbf{r}}, t)\right]^2 \right\},$$

(B1)

with $\hat{\mathbf{A}}_s$ the vector potential describing the photon field, dictates the ionization dynamics of atom A, scattering of the resulting photoelectron wave packet by atom B, collision-induced excitation of the latter, and photoemission upon deexcitation of atom B. The interaction $\hat{\mathbf{V}}_I$, mediating elastic scattering from, as well as excitation of, atom B without change in the distribution of photon modes is defined in Eq. (3b).

We search for a solution, $|\Psi_S(t)\rangle$, satisfying

$$i\frac{\partial}{\partial t}|\Psi_S(t)\rangle = \hat{\mathbf{H}}_{AB}(t)|\Psi_S(t)\rangle.$$

(B2a)

To keep the calculations tractable, we employ a time-dependent perturbative series expansion for

$$|\Psi_S(t)\rangle \approx |\Psi_S^{(0)}(t)\rangle + \sum_{k=1}^{k_{\max}} |\Psi_S^{(k)}(t)\rangle.$$

(B2b)

The zeroth-order term $|\Psi_S^{(0)}(t)\rangle$ describes the isolated atoms A and B in their respective ground states $|\Phi_{\gamma_a^0}^A\rangle$ and $|\Phi_{\gamma_b^0}^B\rangle$ and the photon field in the vacuum state,

$$
\begin{aligned}
\left|\Psi_S^{(0)}(t)\right\rangle &= e^{-i\left(\epsilon_{\gamma_a^0}^A + \epsilon_{\gamma_b^0}^B\right)t} \\
&\times \left[\left|\Phi_{\gamma_a^0}^A\right\rangle \otimes \left|\Phi_{\gamma_b^0}^B\right\rangle - \left|\Phi_{\gamma_b^0}^B\right\rangle \otimes \left|\Phi_{\gamma_a^0}^A\right\rangle\right] \otimes |0\rangle.
\end{aligned}
\tag{B2c}
$$

The phase associated to the zero-point energy has been omitted in Eq. (B2c), as the corresponding phase $\exp[i\hbar\omega_0 t/2]$ cancels out in both sides of the equations when constructing the equations of motion for the expansion coefficients. At intermediate times, $|\Psi_S(t)\rangle$ is written as a coherent superposition in the antisymmetrized tensor product space spanned by the eigenvectors of the isolated Hamiltonians and a coherent multimode photon field,

$$
\begin{aligned}
\left|\Psi_S^{(k+1)}(t)\right\rangle &= \sum_{\gamma_a^A, \gamma_b^B} \sum_{n_{k_1,\sigma_1}} \sum_{n_{k_2,\sigma_2}} \dots \left|\Phi_{\gamma_a^A, \gamma_b^B}\right\rangle \otimes \prod_{k_j,\sigma_j} \left|n_{k_j,\sigma_j}\right\rangle \\
&\times \exp\left\{-i\left[\epsilon_{\gamma_a}^A + \epsilon_{\gamma_b}^B + \sum_{k_i,\sigma_i} \omega(k_i)\, n_{k_i,\sigma_i}\right]t\right\} \\
&\times S_{\gamma_a^A, \gamma_b^B}^{(k+1)}\left(n_{k_1,\sigma_1}, n_{k_2,\sigma_2}, n_{k_3,\sigma_3} \dots; t\right),
\end{aligned}
\tag{B2d}
$$

where $\left|\Phi_{\gamma_a^A, \gamma_b^B}\right\rangle \equiv \left|\Phi_{\gamma_a^A}^A\right\rangle \otimes \left|\Phi_{\gamma_b^B}^B\right\rangle - \left|\Phi_{\gamma_b^B}^B\right\rangle \otimes \left|\Phi_{\gamma_a^A}^A\right\rangle$.

2. Observables

The expansion coefficients in Eq. (B2d) are used to evaluate the angle-resolved correlated probability of photon-pair

emission according to

$$
\frac{d^2\sigma_{n_f}}{d(h\nu_1)\, d\Omega_{\hat{k}_1}} = \int d^3 p_a^A \left|\sum_{k=0}^{k_{\max}} S_{p_a^A, \gamma_b^0}^{(k)}(n_f; t \to \infty)\right|^2,
\tag{B3}
$$

where the incoherent summation (integration) is performed over the momenta of the scattered photoelectron. Ionization of atom B by electron impact is not considered. Thus, at $t \to \infty$, atom B returns to its ground state defined by the quantum numbers $\gamma_{b^0}^B$. At intermediate times, the photon field may be excited following complex emission and absorption dynamics. The photon-field configuration n_f in Eq. (B3) specifies the distribution of the photon modes of interest at $t \to \infty$.

The photon-field configuration corresponding to the radiative two-photon cascade emission depicted in Figs. 1(c) and 2(b) corresponds to the distribution of modes defined by $\mathbf{n}_f = [0, 0, \dots, 1_{m_1}, \dots, 0, \dots, 1_{m_2}, 0, \dots]^T$, where m_2 denotes the mode of photon (2). It is defined by the photon energy $h\nu_2 = 12.078$ eV, polarization component along σ_{2a} in Fig. 2(b), and direction of photodetection defined by the (fixed) angles $\theta_{k_2} = \pi/2$ and $\phi_{k_2} = -\pi/2$ in Fig. 2(b). For additional details, see Sec. C 1 b below. On the other hand, m_1 denotes the photon mode defined by $h\nu_1 = 0.661$ eV, and polarization component along $\sigma_{1b}(\theta_{k_1})$ in Fig. 2(b), as the photon in mode (1) is detected as a function of the angle θ_{k_1}; cf. Sec. C 1 b.

3. Propagation of the time-dependent coefficients

To alleviate the notation, we introduce the occupation number representation $\boldsymbol{n} = [n_1, n_2, \dots n_p \dots]$ describing n_p photons in mode p. Analogously, we define $\boldsymbol{n} \pm \mathbf{1}_p = [n_1, n_2, \dots n_p \pm 1 \dots]$ and $\boldsymbol{n} \pm \mathbf{2}_p = [n_1, n_2, \dots n_p \pm 2 \dots]$ and $|\boldsymbol{n}\rangle = |n_1, n_2, \dots, n_p, \dots\rangle$. The indices run over all photon modes, hereafter referred to as Ω_γ.

The time-dependent expansion coefficients in Eq. (B2d) are obtained by projecting Eq. (B2a) onto $|\Phi_{\gamma_a'^A}^A \Phi_{\gamma_b'^B}^B; \boldsymbol{n}'\rangle$ and iteratively solving the recursive equation

$$
S_{\gamma_a^A, \gamma_b^B}^{(k+1)}(\boldsymbol{n}'; t) = \int_{-\infty}^{t} \left\langle \Phi_{\gamma_a'^A}^A \Phi_{\gamma_b'^B}^B; \boldsymbol{n}' \middle| \tilde{\Psi}^{(k)}(t')\right\rangle dt' + \sum_{\gamma_a^A, \gamma_b^B} \left[S_{\gamma_a^A, \gamma_b^B}^{(k)}(\boldsymbol{n}'; t)\, e^{i\left(\epsilon_{\gamma_a'}^A + \epsilon_{\gamma_b'}^B - \epsilon_{\gamma_a}^A - \epsilon_{\gamma_b}^B\right)t}\right]_{t_0}^{t} \left\langle \Phi_{\gamma_a'^A}^A \middle| \Phi_{\gamma_b}^B\right\rangle \left\langle \Phi_{\gamma_b'^B}^B \middle| \Phi_{\gamma_a}^A\right\rangle,
\tag{B4a}
$$

with $t_0 \to -\infty$. The integrand in Eq. (B4a) reads

$$
\left\langle \Phi_{\gamma_a'^A}^A \Phi_{\gamma_b'^B}^B; \boldsymbol{n}' \middle| \tilde{\Psi}^{(k)}(t')\right\rangle = \prod_{s \in \Omega_\gamma} e^{i\left(\epsilon_{\gamma_a'}^A + \epsilon_{\gamma_b'}^B + \hbar n_s' \omega_s\right)t'} \left\langle \Phi_{\gamma_a^A}^A \Phi_{\gamma_b^B}^B; \boldsymbol{n}' \middle| \hat{\mathbf{H}}_I(t') \middle| \Psi_S^{(k)}(t')\right\rangle.
\tag{B4b}
$$

Here we have defined, upon expansion of the quadratic term in Eq. (B1),

$$
\hat{\mathbf{H}}_I(t) = \left[-e\,\hat{\mathbf{r}} \cdot \hat{\mathbf{E}}(\hat{\mathbf{r}}, t) + V_{ne}^B(\hat{\mathbf{r}} - \boldsymbol{R}_B)\right] \otimes \mathbb{1} + \hat{\mathbf{V}}_{ee}(\hat{\mathbf{r}}, \hat{\mathbf{r}}') + \mathbb{1} \otimes \left[-\frac{e}{mc}\hat{\mathbf{A}}_s(\hat{\mathbf{r}}) \cdot \hat{\mathbf{p}} + \frac{e^2}{2mc}\hat{\mathbf{A}}_s(\hat{\mathbf{r}}) \cdot \hat{\mathbf{A}}_s(\hat{\mathbf{r}})\right],
\tag{B4c}
$$

with $V_{ne}^B(\hat{\mathbf{r}} - \boldsymbol{R}_B) \otimes \mathbb{1}$ the potential-energy interaction between the incident electron and the nuclear charge distribution of atom B, and $\hat{\mathbf{V}}_{ee}(\hat{\mathbf{r}}, \hat{\mathbf{r}}')$ the potential-energy interaction between the incident and the target electron. The second term in Eq. (B4a), proportional to $\langle \Phi_{\gamma_a'^A}^A | \Phi_{\gamma_b}^B\rangle \langle \Phi_{\gamma_b'^B}^B | \Phi_{\gamma_a}^A\rangle$, arises from the antisymmetrization of the two-electron state vector in Eq. (B2d) and may not vanish due to the overlap between the scattering states of A and the bound states of B.

After using Eqs. (B4a), (B4b), and (B1), and carrying out some straightforward algebra, the expression for the expansion coefficients can be recast into the form

$$
\begin{aligned}
S_{\gamma_a'^A, \gamma_b'^B}^{(k+1)}(\boldsymbol{n}'; t) &= C_{[E]}^{(k+1)}\left(\gamma_a'^A, \gamma_b'^B, \boldsymbol{n}'; t\right) + C_{[V_B]}^{(k+1)}\left(\gamma_a'^A, \gamma_b'^B, \boldsymbol{n}'; t\right) + C_{[V_{AB}]}^{(k+1)}\left(\gamma_a'^A, \gamma_b'^B, \boldsymbol{n}'; t\right) \\
&+ C_{[h\nu]}^{(k+1)}\left(\gamma_a'^A, \gamma_b'^B, \boldsymbol{n}'; t\right) + C_{[X]}^{(k+1)}\left(\gamma_a'^A, \gamma_b'^B, \boldsymbol{n}'; t\right).
\end{aligned}
\tag{B4d}
$$

4. Coherent electron-impact dynamics

Defining $\boldsymbol{\gamma}' \equiv (\gamma_a'^A, \gamma_b'^B)$, the first term in Eq. (B4d),

$$C_{[E]}^{(k+1)}(\boldsymbol{\gamma}', \boldsymbol{n}'; t) = ie \sum_{\mu_0, \gamma_a^A} \langle \Phi_{\gamma_a'^A}^A | \hat{\mathbf{r}} \mu_0 f_{\Omega_A}(\hat{\mathbf{r}}) | \Phi_{\gamma_a}^A \rangle$$
$$\times \int_{-\infty}^{t} S_{\gamma_a^A, \gamma_b'^B}^{(k)}(\boldsymbol{n}'; t') e^{i(\epsilon_{\gamma_a'}^A - \epsilon_{\gamma_a}^A)t'} E_{\mu_0}(t') dt',$$

(B5)

accounts for the correction to the expansion coefficients due to the classical field defined in Eq. (A2). The second term,

$$C_{[V_B]}^{(k+1)}(\boldsymbol{\gamma}', \boldsymbol{n}'; t) = -i \sum_{\gamma_a^A} \langle \Phi_{\gamma_a'^A}^A | \hat{\mathbf{V}}_{ne}(\hat{\mathbf{r}} - \boldsymbol{R}_B) | \Phi_{\gamma_a}^A \rangle$$
$$\times \int_{-\infty}^{t} S_{\gamma_a^A, \gamma_b'^B}^{(k)}(\boldsymbol{n}'; t') e^{i(\epsilon_{\gamma_a'}^A - \epsilon_{\gamma_a}^A)t'} dt', \quad \text{(B6)}$$

accounts for the correction to the scattering component $\gamma_a'^A$ of the expansion coefficients due to the potential-energy interaction between the incident electron and the nuclear charge density at $r_{0,B}$, while leaving the component $\gamma_b'^B$ and the photon field unchanged. Next,

$$C_{[V_{AB}]}^{(k+1)}(\boldsymbol{\gamma}', \boldsymbol{n}'; t) = -i \sum_{\gamma_a^A, \gamma_b^B} \langle \Phi_{\gamma_a'^A}^A \Phi_{\gamma_b'^B}^B | \hat{\mathbf{V}}_{ee}(\hat{\mathbf{r}}, \hat{\mathbf{r}}') | \Phi_{\gamma_a}^A \Phi_{\gamma_b}^B \rangle$$
$$\times \int_{-\infty}^{t} S_{\gamma_a^A, \gamma_b^B}^{(k)}(\boldsymbol{n}'; t') e^{i\varphi(\boldsymbol{\gamma}', \gamma_a^A, \gamma_b^B)t'} dt', \quad \text{(B7)}$$

where $\varphi(\boldsymbol{\gamma}', \gamma_a^A, \gamma_b^B) \equiv \epsilon_{\gamma_a'}^A + \epsilon_{\gamma_b'}^B - \epsilon_{\gamma_a}^A - \epsilon_{\gamma_b}^B$, accounts for the interaction between the incident electron and the electron

initially in atom B. More precisely, Eq. (B7) accounts for the elastic and inelastic excitation of atom B triggered by the incident wave packet. It describes, to lowest order, the scattering of an initial continuum-state component along $|\Phi_{\gamma_a}^A\rangle$ to $|\Phi_{\gamma_a'^A}^A\rangle$, leading to excitation of atom B from $|\Phi_{\gamma_b}^B\rangle$ to $|\Phi_{\gamma_a'^B}^B\rangle$ without change in the distribution of photon modes.

5. Single photons and sequentially or simultaneously emitted (absorbed) photon pairs

a. One-photon exchange

Deexcitation of atom B following the excitation triggers the dynamics of photon emission (absorption) dictated by the fourth term in Eq. (B4d). The latter can be split according to the net number of exchanged photons as

$$C_{[h\nu]}^{(k+1)}(\gamma_a'^A, \gamma_b'^B, \boldsymbol{n}'; t) = -i \kappa_{1ph} C_{[1ph]}^{(k+1)}(\boldsymbol{\gamma}', \boldsymbol{n}'; t)$$
$$- i\kappa_{2ph} C_{[2ph]}^{(k+1)}(\boldsymbol{\gamma}', \boldsymbol{n}'; t), \quad \text{(B8)}$$

with $\kappa_{1ph} = -e/mc$ and $\kappa_{2ph} = e^2/2mc$. The first (second) term in Eq. (B8) describes the exchange of one (two) photons. The first term arises from the contribution $\propto \hat{\mathbf{A}}_s(\hat{\mathbf{r}}) \cdot \hat{\mathbf{p}}$ in Eq. (B4c). It can be written as

$$C_{[1ph]}^{(k+1)}(\boldsymbol{\gamma}', \boldsymbol{n}'; t) = W_{[abs]}^{(k+1)}(\boldsymbol{\gamma}', \boldsymbol{n}'; t) + W_{[em]}^{(k+1)}(\boldsymbol{\gamma}', \boldsymbol{n}'; t).$$

(B9)

The two parts in Eq. (B9) dictate the absorption and emission of one net photon according to

$$W_{[abs]}^{(k+1)}(\boldsymbol{\gamma}', \boldsymbol{n}'; t) = \sum_{\gamma_b^B} \sum_{q \in \Omega_\gamma} A_q \sqrt{n_q' + 1} \langle \Phi_{\gamma_b'^B}^B | e^{i\mathbf{k}_q \cdot \hat{\mathbf{r}}} \hat{\mathbf{p}} | \Phi_{\gamma_b}^B \rangle \cdot \boldsymbol{\epsilon}_q \int_{-\infty}^{t} S_{\gamma_a'^A, \gamma_b^B}^{(k)}(\boldsymbol{n}' + \mathbf{1}_q; t') e^{i(\epsilon_{\gamma_b'}^B - \epsilon_{\gamma_b}^B - \hbar\omega_q)t'} dt', \quad \text{(B10a)}$$

$$W_{[em]}^{(k+1)}(\boldsymbol{\gamma}', \boldsymbol{n}'; t) = \sum_{\gamma_b^B} \sum_{q \in \Omega_\gamma} A_q \sqrt{n_q'} \langle \Phi_{\gamma_b'^B}^B | e^{-i\mathbf{k}_q \cdot \hat{\mathbf{r}}} \hat{\mathbf{p}} | \Phi_{\gamma_b}^B \rangle \cdot \boldsymbol{\epsilon}_q \int_{-\infty}^{t} S_{\gamma_a'^A, \gamma_b^B}^{(k)}(\boldsymbol{n}' - \mathbf{1}_q; t') e^{i(\epsilon_{\gamma_b'}^B - \epsilon_{\gamma_b}^B + \hbar\omega_q)t'} dt'. \quad \text{(B10b)}$$

Here we used the convention of Sec. B 3 and defined $A_q = \sqrt{\hbar/2\omega_q\epsilon_0 V_0}$. The photon mode labeled as q is defined by the momentum $\hbar\mathbf{k}_q$ and polarization $\boldsymbol{\epsilon}_q$ of the emitted (absorbed) photon. Emission (absorption) of a photon in mode q yields deexcitation (excitation) of atom B from $|\Phi_{\gamma_b}^B\rangle$ to $|\Phi_{\gamma_b'^B}^B\rangle$. For photon pairs sequentially emitted in a radiative photon-cascade process, the largest contributing term is given by Eq. (B10b), although the dynamics of photoemission may also be affected by additional terms describing absorption and emission involving two-photon exchange processes.

b. Two-photon exchange

The coefficient $C_{[2ph]}^{(k+1)}(\boldsymbol{\gamma}', \boldsymbol{n}'; t)$ in Eq. (B8) arises from the term proportional to $\hat{\mathbf{A}}_s(\hat{\mathbf{r}}) \cdot \hat{\mathbf{A}}_s(\hat{\mathbf{r}})$ in Eq. (B4c). It describes real and virtual two-photon emission (absorption) in the same or different modes with effective two or zero net photon-exchange processes between atom B and the photon field. Compared to its counterpart proportional to κ_{1ph} in Eq. (B8),

this term is $\propto e^2$. Consequently, it provides a weaker contribution to one-step cascade processes. However, it must be taken into account for radiative processes involving two or more optical cascades, as the multiplying factors appearing in powers of e for both terms may become commensurate. We define this term according to whether or not the exchanged photons are in the same or different modes, namely,

$$C_{[2ph]}^{(k+1)}(\boldsymbol{\gamma}', \boldsymbol{n}'; t) = P^{(k+1)}(\boldsymbol{\gamma}', \boldsymbol{n}'; t) + Q^{(k+1)}(\boldsymbol{\gamma}', \boldsymbol{n}'; t).$$

(B11)

The first (second) term in Eq. (B11) describes the exchange of two photons in the same (or different) mode(s). The first term in Eq. (B11) may be decomposed as

$$P^{(k+1)}(\boldsymbol{\gamma}', \boldsymbol{n}'; t) = P_{[em,em]}^{(k+1)}(\boldsymbol{\gamma}', \boldsymbol{n}'; t) + P_{[abs,abs]}^{(k+1)}(\boldsymbol{\gamma}', \boldsymbol{n}'; t)$$
$$+ P_{[em,abs]}^{(k+1)}(\boldsymbol{\gamma}', \boldsymbol{n}'; t), \quad \text{(B12)}$$

where we have defined (using $|\Phi^B_{\gamma^B_b}\rangle \equiv |\Phi^B_{\gamma_b}\rangle$)

$$P^{(k+1)}_{[abs,abs]}(\gamma', \boldsymbol{n}'; t) = \sum_{\gamma^B_b} \sum_{q \in \Omega_\gamma} A_q A_q \langle \Phi^B_{\gamma'_b} | e^{2i\mathbf{k}_q \cdot \hat{\mathbf{r}}} | \Phi^B_{\gamma_b} \rangle \sqrt{n_q + 1} \sqrt{n_q + 2} \int_{-\infty}^t S^{(k)}_{\gamma'^A_a, \gamma^B_b}(\boldsymbol{n}' + \boldsymbol{2}_q; t') e^{i(\epsilon^B_{\gamma'_b} - \epsilon^B_{\gamma_b} - 2\hbar\omega_q)t'} dt', \quad \text{(B13a)}$$

$$P^{(k+1)}_{[em,em]}(\gamma', \boldsymbol{n}'; t) = \sum_{\gamma^B_b} \sum_{q \in \Omega_\gamma} A_q A_q \langle \Phi^B_{\gamma'_b} | e^{-2i\mathbf{k}_q \cdot \hat{\mathbf{r}}} | \Phi^B_{\gamma_b} \rangle \sqrt{n'_q - 1} \sqrt{n'_q} \int_{-\infty}^t S^{(k)}_{\gamma'^A_a, \gamma^B_b}(\boldsymbol{n}' - \boldsymbol{2}_q; t') e^{i(\epsilon^B_{\gamma'_b} - \epsilon^B_{\gamma_b} + 2\hbar\omega_q)t'} dt', \quad \text{(B13b)}$$

$$P^{(k+1)}_{[em,abs]}(\gamma', \boldsymbol{n}'; t) = \sum_{q \in \Omega_\gamma} A_q A_q (2n'_q + 1) \int_{-\infty}^t S^{(k)}_{\gamma'^A_a, \gamma^B_b}(\boldsymbol{n}'; t') dt'. \quad \text{(B13c)}$$

Equation (B13a) describes the absorption of two photons in the same mode q and subsequent excitation of atom B from $|\Phi^B_{\gamma^B_b}\rangle$ to $|\Phi^B_{\gamma'^B_b}\rangle$, leaving the scattered photoelectron unaffected if two photons in the same mode q are present in the field at the previous iteration step (k), and if the state $|\Phi^B_{\gamma^B_b}\rangle$ is populated. The distribution of modes then goes from $\boldsymbol{n}' + \boldsymbol{2}_q$ to n'_q photons in mode q, i.e., compare the terms $S^{(k)}_{\gamma'^A_a, \gamma^B_b}(\boldsymbol{n}' + \boldsymbol{2}_q; t')$ (uncorrected) and $P^{(k+1)}_{[em,em]}(\gamma', \boldsymbol{n}'; t)$ (corrected).

Next, Eq. (B13b) accounts for the emission of two photons in the same mode q. For $k_q r \ll 1$, the description of excitation (deexcitation) induced by simultaneous two-photon absorption (emission) requires both terms to be treated beyond the dipole approximation. Note that the emission and absorption of photons may occur without excitation (deexcitation), even in the dipole approximation. Simultaneous emission of a photon in mode q and absorption of a photon in the same mode with no electron dynamics involved is described by Eq. (B13c).

Finally, the second term in Eq. (B11), describing the simultaneous exchange of two photons in different modes, reads

$$Q^{(k+1)}(\gamma', \boldsymbol{n}'; t) = Q^{(k+1)}_{[abs,abs]}(\gamma', \boldsymbol{n}'; t) + Q^{(k+1)}_{[em,em]}(\gamma', \boldsymbol{n}'; t) + Q^{(k+1)}_{[em,abs]}(\gamma', \boldsymbol{n}'; t), \quad \text{(B14)}$$

where, in analogy with Eq. (B13), we have defined

$$Q^{(k+1)}_{[abs,abs]}(\gamma', \boldsymbol{n}'; t) = \sum_{\gamma^B_b} \sum_{\substack{p, q \in \Omega \\ p \neq q}} A^p_q(n'_p + 1, n'_q + 1) \langle \Phi^B_{\gamma'_b} | e^{i(\mathbf{k}_p + \mathbf{k}_q) \cdot \hat{\mathbf{r}}} | \Phi^B_{\gamma_b} \rangle \int_{-\infty}^t S^{(k)}_{\gamma'^A_a, \gamma^B_b}(\boldsymbol{n}' + \boldsymbol{1}_p + \boldsymbol{1}_q; t') e^{i[\epsilon^B_{\gamma'_b} - \epsilon^B_{\gamma_b} - \hbar(\omega_p + \omega_q)]t'} dt',$$

$$\text{(B15a)}$$

$$Q^{(k+1)}_{[em,em]}(\gamma', \boldsymbol{n}'; t) = \sum_{\gamma^B_b} \sum_{\substack{p, q \in \Omega \\ p \neq q}} A^p_q(n'_p, n'_q) \langle \Phi^B_{\gamma'_b} | e^{-i(\mathbf{k}_p + \mathbf{k}_q) \cdot \hat{\mathbf{r}}} | \Phi^B_{\gamma_b} \rangle \int_{-\infty}^t S^{(k)}_{\gamma'^A_a, \gamma^B_b}(\boldsymbol{n}' + \boldsymbol{1}_p + \boldsymbol{1}_q; t') e^{i[\epsilon^B_{\gamma'_b} - \epsilon^B_{\gamma_b} + \hbar(\omega_p + \omega_q)]t'} dt',$$

$$\text{(B15b)}$$

$$Q^{(k+1)}_{[abs,em]}(\gamma', \boldsymbol{n}'; t) = \sum_{\gamma^B_b} \sum_{\substack{p, q \in \Omega \\ p \neq q}} A^p_q(n'_p + 1, n'_q) \langle \Phi^B_{\gamma'_b} | e^{i(\mathbf{k}_p - \mathbf{k}_q) \cdot \hat{\mathbf{r}}} | \Phi^B_{\gamma_b} \rangle \int_{-\infty}^t S^{(k)}_{\gamma'^A_a, \gamma^B_b}(\boldsymbol{n}' + \boldsymbol{1}_p + \boldsymbol{1}_q; t') e^{i[\epsilon^B_{\gamma'_b} - \epsilon^B_{\gamma_b} + \hbar(\omega_q - \omega_p)]t'} dt',$$

$$\text{(B15c)}$$

with $A^p_q(n'_p, n'_q) = A_p A_q \sqrt{n'_p} \sqrt{n'_q}\, (\mathbf{e}_p \cdot \mathbf{e}_q)$. Equation (B15a) accounts for the simultaneous absorption of two photons in different modes, while Eq. (B15b) describes the simultaneous emission of two photons in different modes. Finally, Eq. (B15c) accounts for the exchange of photon pairs without a net change in the photon number: it describes the simultaneous absorption and emission of one photon in different modes. The matrix elements and angular distributions involving simultaneously emitted (absorbed) photon pairs are evaluated following the prescription given in Sec. C 2 b.

For the photon wavelengths considered in this work, the contribution due to the term $\hat{\mathbf{A}}_s(\hat{\mathbf{r}}) \cdot \hat{\mathbf{A}}_s(\hat{\mathbf{r}})$ driving *simultaneous photon-pair emission* via optical deexcitation is expected to be less important compared to the case of *sequential photon-pair emission* mediated by the term $\hat{\mathbf{A}}_s(\hat{\mathbf{r}}) \cdot \hat{\mathbf{p}}$, since the matrix elements corresponding to the former would vanish in the dipole approximation. It is worth mentioning that Eq. (B10b) or, more specifically, a two-step sequential application of Eq. (B10b) provides the leading contribution to the emission of photon pairs with energies $h\nu_1$ and $h\nu_2$: the correlated photon pair originates from sequential emission from the target atom B, following the deexcitation pathways depicted in Fig. 1(c).

6. Exchange term $C_{[X]}^{(k+1)}(\gamma_a'^A, \gamma_b'^B, n'; t)$

Finally, proper antisymmetrization of the two-electron wave function is ensured by the last term in Eq. (B4d): $C_{[X]}^{(k+1)}(\gamma_a'^A, \gamma_b'^B, n'; t)$. The latter updates the expansion coefficients to ensure the required exchange symmetry via the iterative correction,

$$
\begin{aligned}
C_{[X]}^{(k+1)}\big(\gamma_a'^A, \gamma_b'^B, \boldsymbol{n}'; t\big) &= i \sum_{\gamma_a^A, \gamma_b^B} \big\langle \Phi_{\gamma_a'^A}^A \big| \hat{\mathbf{V}}_{ne}(\hat{\mathbf{r}} - R_B) \big| \Phi_{\gamma_b^B}^B \big\rangle \big\langle \Phi_{\gamma_b'^B}^B \big| \Phi_{\gamma_a^A}^A \big\rangle \int_{-\infty}^{t} S_{\gamma_a^A, \gamma_b^B}^{(k)}(\boldsymbol{n}'; t') e^{i(\epsilon_{\gamma_a'}^A + \epsilon_{\gamma_b'}^B - \epsilon_{\gamma_a}^A - \epsilon_{\gamma_b}^B) t'} \, dt' \\[4pt]
&\quad + i \sum_{\gamma_a^A, \gamma_b^B} \big\langle \Phi_{\gamma_a'^A}^A \Phi_{\gamma_b'^B}^B \big| \hat{\mathbf{V}}_{ee}(\hat{\mathbf{r}}, \hat{\mathbf{r}}') \big| \Phi_{\gamma_b^B}^B \Phi_{\gamma_a^A}^A \big\rangle \int_{-\infty}^{t} S_{\gamma_a^A, \gamma_b^B}^{(k)}(\boldsymbol{n}'; t') e^{i(\epsilon_{\gamma_a'}^A + \epsilon_{\gamma_b'}^B - \epsilon_{\gamma_a}^A - \epsilon_{\gamma_b}^B) t'} \, dt' \\[4pt]
&\quad - \sum_{\gamma_a^A} \underline{\underline{C}}_{[h\nu]}^{(k+1)}\big(\gamma_a^A, \gamma_b'^B, \boldsymbol{n}'; t\big) + \sum_{\gamma_a^A, \gamma_b^B} \mathcal{O}_{\gamma_a^A, \gamma_b^B}^{\gamma_a'^A, \gamma_b'^B} \Big[S_{\gamma_a^A, \gamma_b^B}^{(k)}(\boldsymbol{n}'; t') e^{(\epsilon_{\gamma_a'}^A + \epsilon_{\gamma_b'}^B - \epsilon_{\gamma_a}^A - \epsilon_{\gamma_b}^B) t'} \Big]_{-\infty}^{t}, \qquad \text{(B16a)}
\end{aligned}
$$

where the overlap matrix, already appearing in Eq. (B4a), reads

$$
\mathcal{O}_{\gamma_a^A, \gamma_b^B}^{\gamma_a'^A, \gamma_b'^B} = \big\langle \Phi_{\gamma_a'^A}^A \big| \Phi_{\gamma_b^B}^B \big\rangle \big\langle \Phi_{\gamma_b'^B}^B \big| \Phi_{\gamma_a^A}^A \big\rangle. \qquad \text{(B16b)}
$$

The double underline in the third term in Eq. (B16a) indicates that the expressions $(\epsilon_{\gamma_b'}^B - \epsilon_{\gamma_b}^B)$ as well as all transition matrix elements of the form $\langle \Phi_{\gamma_b'^B}^B | \mathcal{T} | \Phi_{\gamma_b^B}^B \rangle$ appearing though Eqs. (B10a)–(B15c) must be replaced with $(\epsilon_{\gamma_a'}^A + \epsilon_{\gamma_b'}^B - \epsilon_{\gamma_a}^A + \epsilon_{\gamma_b}^B)$ and $\langle \Phi_{\gamma_b'^B}^B | \mathcal{T} | \Phi_{\gamma_a^A}^A \rangle \langle \Phi_{\gamma_a'^A}^A | \Phi_{\gamma_b^B}^B \rangle$, respectively. Note that the classical field does not contribute to the exchange term because of $f_{\Omega_A}(r)$ and the localized character of $\mathcal{H}_B$, i.e., the expansion coefficients vanish for the continuum states of atom B: ionization of atom B by electron impact is not considered. The maximum number of sequential radiative cascade steps describing the deexcitation pathways from an excited state to the ground state is determined by the maximum order in the perturbation expansion, $k_{\max}$. The reported results were obtained by iterating the expansion coefficients up to $k_{\max} = 6$, corresponding to the lowest order needed to describe the process of radiative two-photon cascade emission while considering the feedback effects of the emitted photons on the scattered electron wave packet.

APPENDIX C: POLARIZATION STATES AND PROPAGATION DIRECTION OF EMITTED (ABSORBED) PHOTONS

1. Transversality condition and polarization components

a. General scheme

Throughout the text, we used the shorthand notation

$$
\boldsymbol{\sigma}_j \equiv (\sigma_{ja}, \sigma_{jb}), \qquad \text{(C1)}
$$

when referring to the indices of the two mutually orthogonal polarization components $\hat{\epsilon}_{\sigma_{ja}}$ and $\hat{\epsilon}_{\sigma_{jb}}$ satisfying the transversality conditions

$$
\hat{\epsilon}_{\boldsymbol{\sigma}_j} \cdot \mathrm{k}_j = 0. \qquad \text{(C2)}
$$

Within this convention, summation over the indices $\boldsymbol{\sigma}_j$, e.g., in Eq. (B2d), implies summation over their components in Eq. (C1) for each momentum $\hbar \mathrm{k}_j$. To construct $\epsilon_{\boldsymbol{\sigma}_j}$ or, equivalently, $\epsilon_{\sigma_{ja}}$ and $\epsilon_{\sigma_{jb}}$ satisfying Eq. (C2), we write k_j in polar coordinates,

$$
\mathrm{k}_j = \sqrt{\frac{4\pi}{3}} \left(\frac{\omega_j}{c} \right) \sum_{q=0,\pm 1} \mathrm{Y}_q^1(\theta_{k_j}, \phi_{k_j}) \, \hat{\mathrm{e}}_q^*, \qquad \text{(C3)}
$$

with $\mathrm{Y}_q^1(\theta_{k_j}, \phi_{k_j})$ as the spherical harmonic for the propagation direction of the mode $(\mathrm{k}_j, \boldsymbol{\sigma}_j)$ and $\hat{\mathrm{e}}_q$ denoting the covariant spherical unit vectors $\mathbf{e}_{-1} = (\mathbf{e}_x - i\mathbf{e}_y)/\sqrt{2}$, $\mathbf{e}_{+1} = -(\mathbf{e}_x + i\mathbf{e}_y)/\sqrt{2}$, and $\mathbf{e}_0 = \mathbf{e}_z$. We then construct the

orthogonal triad of unit vectors $(\mathrm{k}_j/|\mathrm{k}_j|, \epsilon_{\sigma_{jq}}, \epsilon_{\sigma_{jq}})$ as

$$
\begin{aligned}
\hat{\epsilon}_{\sigma_{ja}} &= \frac{\mathrm{k}_j \times \hat{\mathrm{e}}_0}{|\mathrm{k}_j \times \hat{\mathrm{e}}_0|} = \frac{1}{\sqrt{2}} \big[i \cos(\theta_{k_j}) - \sin(\phi_{k_j}) \big] \mathrm{e}_{+1} \\
&\quad + \frac{1}{\sqrt{2}} \big[i \cos(\theta_{k_j}) + \sin(\phi_{k_j}) \big] \mathrm{e}_{-1}, \qquad \text{(C4)}
\end{aligned}
$$

for the first polarization component, and

$$
\begin{aligned}
\hat{\epsilon}_{\sigma_{jb}} &= \frac{\mathrm{k}_j \times \hat{\epsilon}_{\sigma_{ja}}}{|\mathrm{k}_j \times \hat{\epsilon}_{\sigma_{ja}}|} \\
&= -\frac{1}{\sqrt{2}} \big[i \sin(\phi_{k_j}) \cos(\theta_{k_j}) + \cos(\phi_{k_j}) \cos(\theta_{k_j}) \big] \mathrm{e}_{+1} \\
&\quad - \frac{1}{\sqrt{2}} \big[i \sin(\phi_{k_j}) \cos(\theta_{k_j}) - \cos(\phi_{k_j}) \cos(\theta_{k_j}) \big] \mathrm{e}_{-1} \\
&\quad - \sin(\theta_{k_j}) \mathrm{e}_0, \qquad \text{(C5)}
\end{aligned}
$$

for the second polarization component, with $(\times)$ denoting the vector cross product. They both fulfill the transversality condition $\hat{\boldsymbol{\epsilon}}_{\boldsymbol{\sigma}_j} \cdot \mathrm{k}_j = 0$.

In Cartesian coordinates, $[\hat{\boldsymbol{e}}_x, \hat{\boldsymbol{e}}_y, \hat{\boldsymbol{e}}_y]$, $\epsilon_{\sigma_{ja}}$ and $\epsilon_{\sigma_{jb}}$ are

$$
\hat{\epsilon}_{\sigma_{ja}} \equiv \begin{bmatrix} \sin(\phi_{k_j}) \\ -\cos(\phi_{k_j}) \\ 0 \end{bmatrix}; \quad \hat{\epsilon}_{\sigma_{jb}} \equiv \begin{bmatrix} \cos(\phi_{k_j}) \cos(\theta_{k_j}) \\ -\sin(\phi_{k_j}) \cos(\theta_{k_j}) \\ -\sin(\theta_{k_j}) \end{bmatrix}. \quad \text{(C6)}
$$

b. Application to the correlated photodetection scheme

Following the photodetection scheme of Fig. 2(b), a photon in mode (2) is detected at the fixed angles $\theta_{k_2} = \pi/2$ and $\phi_{k_2} =$

$-\pi/2$. This gives, according to Eq. (C6), $\epsilon_{\sigma_{2a}} = [-1, 0, 0]$ and $\epsilon_{\sigma_{2b}} = [0, 0, -1]$. The first detector $\mathcal{D}_2$ measures the photon with energy $h\nu_2$ with polarization component along $\epsilon_{\sigma_{2b}}$, i.e., along $\hat{z}$.

A second detector $\mathcal{D}_1$ detects the photon with energy $h\nu_1$ at fixed $\phi_{k_1} = \pi/2$, but it is free to move and hence scan along θ_{k_1}. According to Eq. (C6), this corresponds to $\epsilon_{\sigma_{1a}} = [1, 0, 0]$ and $\epsilon_{\sigma_{1b}} = [0, -\cos(\theta_{k_1}), -\sin(\theta_{k_1})]$. The detector $\mathcal{D}_1$ measures the correlated photon pair with energy $h\nu_1$ with the polarization component along $\epsilon_{\sigma_{1b}}$ as it scans along θ_{k_1}.

2. Angular distributions and transition matrix elements

a. Angular distributions of single photons and sequentially emitted (absorbed) photon pairs

The directions of propagation of the emitted (absorbed) photons are evaluated by means of a multipole expansion of the exponential terms, $\exp(ikr)$, which appear in the matrix elements of the expansion coefficients defined throughout

Sec. B 5. Specifically,

$$e^{\pm i\mathbf{k}_j \cdot \mathbf{r}} = 4\pi \sum_{\lambda,\mu} (\pm i)^\lambda j_\lambda(k_j r) Y_\mu^\lambda(\theta_r, \phi_r) Y_\mu^{\lambda*}(\theta_{k_j}, \phi_{k_j}), \quad \text{(C7)}$$

where $j_\lambda(k_j r)$ denotes a spherical Bessel function. For the photon energies considered in this work, the wavelengths defining the modes emitted and absorbed during the propagation of the expansion coefficients are several orders of magnitude larger than the extension of the most diffuse bound state of the target atom B. The Bessel functions can therefore be approximated by

$$j_\lambda(k_j r) \approx (k_j r)^\lambda / (2\lambda + 1)!!, \quad \text{(C8)}$$

since $k_j r \ll 1$. This allows us to obtain the transition matrix elements as a power series in r^λ. Following this prescription, the matrix elements defined in Eqs. (B10a) and (B10b) are given by

$$\langle \Phi_{\gamma_b'^{B}}^B | e^{\pm \mathbf{k}_j \cdot \hat{\mathbf{r}}} \hat{\mathbf{p}}_{\mu_0} | \Phi_{\gamma_b^B}^B \rangle = \sum_{\lambda,\mu} \langle \Phi_{\gamma_b'^B}^B | \mathcal{D}_{\mu,\mu_0}^{[\lambda,\pm]}(k_j) | \Phi_{\gamma_b^B}^B \rangle Y_\mu^{\lambda*}(\Omega_{k_j}), \quad \text{(C9a)}$$

with $\Omega_{k_j} \equiv (\theta_{k_j}, \phi_{k_j})$. The multipole coefficients are obtained by standard angular-momentum techniques as

$$\langle \Phi_{\gamma_b'^B}^B | \mathcal{D}_{\mu,\mu_0}^{[\lambda,\pm]}(k_j) | \Phi_{\gamma_b^B}^B \rangle$$

$$= C \frac{(\pm i)^\lambda (k_j)^\lambda}{(2\lambda + 1)!!} (-1)^{l'+m'} \sum_{q=|l'-\lambda|}^{l'+\lambda} \left[\frac{(2l'+1)(2\lambda+1)}{1/(2q+1)} \right]^{\frac{1}{2}} \begin{pmatrix} l' & \lambda & q \\ -m' & \mu & m+\mu_0 \end{pmatrix} \begin{pmatrix} l' & \lambda & q \\ 0 & 0 & 0 \end{pmatrix} \delta_{m'-\mu, m+\mu_0}$$

$$\times \begin{cases} \int_0^{+\infty} r^{\lambda+2} f_{n',l'}(r) \left(\frac{\partial}{\partial r} - \frac{l}{r} \right) f_{n,l}(r) dr \left[\left(\frac{l+1}{2l+3} \right)^{\frac{1}{2}} (-1)^{l-1+m+\mu_0} \begin{pmatrix} l & 1 & l+1 \\ m & \mu_0 & -m-\mu_0 \end{pmatrix} \right] \delta_{q,l+1} \\ -\int_0^{+\infty} r^{\lambda+2} f_{n',l'}(r) \left(\frac{\partial}{\partial r} + \frac{l}{r} \right) f_{n,l}(r) dr \left[\left(\frac{l}{2l-1} \right)^{\frac{1}{2}} (-1)^{l-1+m+\mu_0} \begin{pmatrix} l & 1 & l-1 \\ m & \mu_0 & m+\mu_0 \end{pmatrix} \right] \delta_{q,l-1} \end{cases}, \quad \text{(C9b)}$$

with $C = -i\hbar\sqrt{36\pi}$. Furthermore, (n', l', m') and (n, l, m) denote the quantum numbers corresponding to $\gamma_b'^B$ and γ_b^B, while $f_{n',l'}(r)$ and $f_{n,l}(r)$ are the radial components of the orbital wave functions $\langle \mathbf{r} | \Phi_{\gamma_b'^B}^B \rangle$ and $\langle \mathbf{r} | \Phi_{\gamma_b^B}^B \rangle$, respectively.

b. Angular distributions of simultaneously emitted (absorbed) photon pairs

Analogously, the matrix elements describing simultaneous two-photon exchange, i.e., emission ($s = -1$) or absorption ($s = +1$) of a photon in mode q_s with momentum $\hbar\mathbf{k}_s$ and emission ($s' = -1$) or absorption ($s' = +1$) of another photon in mode $q_{s'}$ with momentum $\hbar\mathbf{k}_{s'}$, such as those appearing in Eqs. (B15), are obtained according to the multipole expansion involving the product of two spherical harmonics. Specifically,

$$\langle \Phi_{\gamma_b'^B}^B | e^{i(s\mathbf{k}_s + s'\mathbf{k}_{s'}) \cdot \hat{\mathbf{r}}} | \Phi_{\gamma_b^B}^B \rangle = \sum_{\substack{\lambda_{s'}, \mu_{s'} \\ \lambda_s, \mu_s}} \langle \Phi_{\gamma_b'^B}^B | \mathcal{O}_{\mu_s,\mu_{s'}}^{[\lambda_s,\lambda_{s'}]}(\boldsymbol{v}_s^{s'}) | \Phi_{\gamma_b^B}^B \rangle Y_{\mu_s}^{\lambda_s*}(\Omega_{k_s}) Y_{\mu_{s'}}^{\lambda_{s'}*}(\Omega_{k_{s'}}), \quad \text{(C10a)}$$

where we have defined $\boldsymbol{v}_s^{s'} \equiv [k_s, s, k_s', s']$. The coefficients are again obtained after straightforward angular-momentum algebra. The result is

$$\langle \Phi_{\gamma_b'^B}^B | \mathcal{O}_{\mu_s,\mu_{s'}}^{[\lambda_s,\lambda_{s'}]}(\boldsymbol{v}_s^{s'}) | \Phi_{\gamma_b^B}^B \rangle = (4\pi)^2 \frac{(is)^{\lambda_s} (is')^{\lambda_{s'}}}{(2\lambda_s + 1)!! (2\lambda_{s'} + 1)!!} \frac{(k_s k_{s'})^{\lambda_s + \lambda_{s'}}}{} (-1)^{l'+m'-\mu_s-\mu_{s'}} \int_0^{+\infty} f_{n',l'}(r) r^{\lambda_s + \lambda_{s'} + 2} f_{n,l}(r) dr$$

$$\times \sum_{\Lambda=|\lambda_s-\lambda_{s'}|}^{\lambda_s+\lambda_{s'}} (-1)^\Lambda \begin{pmatrix} \lambda_s & \lambda_{s'} & \Lambda \\ \mu_s & \mu_{s'} & -\mu_s-\mu_{s'} \end{pmatrix} \begin{pmatrix} \lambda_s & \lambda_{s'} & \Lambda \\ 0 & 0 & 0 \end{pmatrix} \begin{pmatrix} l' & \Lambda & l \\ -m' & \mu_s+\mu_{s'} & m \end{pmatrix} \begin{pmatrix} l' & \Lambda & l \\ 0 & 0 & 0 \end{pmatrix}$$

$$\times \left[\frac{(2\lambda_s + 1)(2\lambda_{s'} + 1)}{4\pi/(2\Lambda+1)} \right]^{\frac{1}{2}} \delta_{m'-m, \mu_s+\mu_{s'}}. \quad \text{(C10b)}$$

[1] D. Tannor and S. Rice, J. Chem. Phys. **83**, 5013 (1985).

[2] M. Shapiro and P. Brumer, *Quantum Control of Molecular Processes* (Wiley, New York, 2012).

[3] M. Shapiro and P. Brumer, Rep. Prog. Phys. **66**, 859 (2003).

[4] Y.-Y. Yin, C. Chen, D. S. Elliott, and A. V. Smith, Phys. Rev. Lett. **69**, 2353 (1992).

[5] K.-J. Yuan and A. D. Bandrauk, J. Phys. B **49**, 065601 (2016).

[6] A. N. Grum-Grzhimailo, E. V. Gryzlova, E. I. Staroselskaya, J. Venzke, and K. Bartschat, Phys. Rev. A **91**, 063418 (2015).

[7] A. N. Grum-Grzhimailo, E. V. Gryzlova, E. I. Staroselskaya, S. I. Strakhova, J. Venzke, N. Douguet, and K. Bartschat, J. Phys.: Conf. Ser. **635**, 012008 (2015).

[8] N. Douguet, A. N. Grum-Grzhimailo, E. V. Gryzlova, E. I. Staroselskaya, J. Venzke, and K. Bartschat, Phys. Rev. A **93**, 033402 (2016).

[9] E. V. Gryzlova, A. N. Grum-Grzhimailo, E. I. Staroselskaya, N. Douguet, and K. Bartschat, Phys. Rev. A **97**, 013420 (2018).

[10] P. V. Demekhin, A. N. Artemyev, A. Kastner, and T. Baumert, Phys. Rev. Lett. **121**, 253201 (2018).

[11] M. Wollenhaupt, A. Assion, D. Liese, C. Sarpe-Tudoran, T. Baumert, S. Zamith, M. A. Bouchene, B. Girard, A. Flettner, U. Weichmann, and G. Gerber, Phys. Rev. Lett. **89**, 173001 (2002).

[12] R. E. Goetz, C. P. Koch, and L. Greenman, Phys. Rev. Lett. **122**, 013204 (2019).

[13] M. Wollenhaupt, C. Lux, M. Krug, and T. Baumert, ChemPhysChem **14**, 1297 (2013).

[14] S. Kerbstadt, K. Eickhoff, T. Bayer, and M. Wollenhaupt, Adv. Phys.: X **4**, 1672583 (2019).

[15] M. Wollenhaupt and T. Baumert, Faraday Discuss. **153**, 9 (2011).

[16] J. F. Clauser, Phys. Rev. D **9**, 853 (1974).

[17] C.-Y. Lu, D. E. Browne, T. Yang, and J.-W. Pan, Phys. Rev. Lett. **99**, 250504 (2007).

[18] X.-Q. Zhou, P. Kalasuwan, T. C. Ralph, and J. L. O'brien, Nat. Photon. **7**, 223 (2013).

[19] P. G. Kwiat, K. Mattle, H. Weinfurter, A. Zeilinger, A. V. Sergienko, and Y. Shih, Phys. Rev. Lett. **75**, 4337 (1995).

[20] X. Guo, C.-l. Zou, C. Schuck, H. Jung, R. Cheng, and H. X. Tang, Light: Sci. Appl. **6**, e16249 (2017).

[21] E. Paspalakis and P. L. Knight, Phys. Rev. Lett. **81**, 293 (1998).

[22] T. Quang, M. Woldeyohannes, S. John, and G. S. Agarwal, Phys. Rev. Lett. **79**, 5238 (1997).

[23] F. Ghafoor, S.-Y. Zhu, and M. S. Zubairy, Phys. Rev. A **62**, 013811 (2000).

[24] X. Sun, B. Zhang, and X. Jiang, Eur. Phys. J. D **55**, 699 (2009).

[25] Y. Jeronimo-Moreno and A. B. U'Ren, Phys. Rev. A **79**, 033839 (2009).

[26] L. Hutter, G. Lima, and S. P. Walborn, Phys. Rev. Lett. **125**, 193602 (2020).

[27] V. Weisskopf and E. Wigner, in *Part I: Particles and Fields. Part II: Foundations of Quantum Mechanics* (Springer, New York, 1997), pp. 30–49.

[28] O. Zatsarinny, Comput. Phys. Commun. **174**, 273 (2006).